OH Radical Gas Phase Reactions with Aliphatic Ethers: A Variational Transition State Theory Study

Claudia Zavala-Oseguera,[†] Juan R. Alvarez-Idaboy,[‡] Gabriel Merino,*[,†] and Annia Galano*[,§]

Departamento de Química, Universidad de Guanajuato, Noria Alta s/n C.P. 36050, Guanajuato, Gto. México, Facultad de Química, Departamento de Física y Química Teórica, Universidad Nacional Autónoma de México, México DF 04510, and Departamento de Química, Universidad Autónoma Metropolitana-Iztapalapa, San Rafael Atlixco 186, Col. Vicentina, Iztapalapa, C. P. 09340, México

Received: June 30, 2009; Revised Manuscript Received: October 21, 2009

A theoretical study of the mechanism and kinetics of the OH radical reactions with aliphatic ethers is presented. Several methods were evaluated using the 6-311++G(d,p) basis set, with dimethyl ether as a test molecule. On the basis of the dimethyl ether results, the M05−2X functional was selected for the rest of the calculations. All the possible H abstraction paths have been modeled, and the importance of differentiating among H atoms bonded to the same C atom, according to their orientation with respect to the O atom in the ether, is analyzed. The rate coefficients are calculated using interpolated variational transition-state theory by mapping (IVTST-M), within the IVTST-M-4/4 scheme, in conjunction with small-curvature tunneling (SCT) corrections. The discussion is focused on the 280−400 K temperature range, but additional information is provided for an extended range (280−2000 K). Our analysis suggests a stepwise mechanism involving the formation of H bonded complexes in the entrance and exit channels. The vicinity of the O atom was found to increase the relative site reactivity. In fact, it was found to influence reactivity to a larger extent than the nature of the carbon site (primary, secondary, or tertiary). The overall agreement between the calculated and the available experimental data is very good and supports the reliability of the rate coefficients and the branching ratios proposed here for the first time. It also supports the performance of the M05−2X functional and the IVTST-M-4/4 scheme for kinetic calculations.

Introduction

Ethers are oxygenated compounds of general formula R_1-O-R_2. They are widely used worldwide, mainly as solvents and as motor fuel additives. They are added to unleaded gasoline to increase the octane rating and to reduce the amounts of toxic emissions from exhausts.[1] Ethers can also be used as fuel additives for biodiesel to improve the engine performance and emission characteristics.[2] Accordingly, they are released into the atmosphere in substantial amounts. Their massive use, combined with their high water solubility, low soil adsorption, and minor biodegradability, makes their emission into the atmosphere, as well as their fate after emission, the focus of environmental concerns. Their main atmospheric loss processes are expected to be their reactions with hydroxyl radicals, as for many other volatile organic compounds (VOC).[3,4] In the particular case of ethers, the competing processes (photolysis,[5] reaction with O_3,[6] and reaction with NO_3 radicals[7]) are negligibly slow.

Dimethyl ether (DME) is one of the most studied ethers from both experimental[8−16] and theoretical[17,18] approaches, when reacting with OH radicals. The reported rate coefficients at room temperature range from 2.36×10^{-12} to 2.99×10^{-12} $cm^3 \cdot molecule^{-1} \cdot s^{-1}$, and the Arrhenius activation energies (E_a) vary from 0.43 to 0.98 $kcal \cdot mol^{-1}$. Due to the DME structure, only one reaction product can be observed: the CH_3-O-CH_2 radical.

Methylethylether (MEE) is the smallest ether with more than one different reaction site, therefore branching ratios and relative site reactivity become important for its reaction with •OH. Unfortunately, there are no products analyses reported for this reaction; in fact, there is scarce available information on it. There is only one experimental report on the MEE + OH reaction,[19] performed in the 274−345 K temperature range and using a relative rate technique. In this range the overall rate coefficient was found to vary little with temperature. Therefore no activation energies were reported, and an average value of 6.59×10^{-12} $cm^3 \cdot molecule^{-1} \cdot s^{-1}$ was proposed. Very recently, Yang et al.[20] studied this reaction using density functional theory (DFT), in particular B3LYP/6-311G(d,p), over a wide temperature range (200−2000 K). These authors proposed an overall rate constant of 5.00×10^{-12} $cm^3 \cdot molecule^{-1} \cdot s^{-1}$ and a negative E_a equal to −0.60 $kcal \cdot mol^{-1}$. No branching ratios were reported since the H abstraction was assumed to take place from the secondary carbon, based on bond dissociation energies and barrier heights considerations.

Even though experimental data for the diethylether (DEE) + OH reaction,[11,12,14,15,21,22] are abundant, there is no information on the branching ratios for this reaction. Its rate constant, at 298 K, ranges from 1.13×10^{-11} to 1.38×10^{-11} $cm^3 \cdot molecule^{-1} \cdot s^{-1}$. All reported Arrhenius activation energies are negative, ranging from −0.23 to −0.54 $kcal \cdot mol^{-1}$. No previous theoretical studies on this reaction have been reported. For the OH reaction with methyl-*n*-propylether (MnPE), methyl-*i*-propylether (MiPE), and methyl-*i*-butylether (MiBE) there is no kinetic data reported, neither experimental nor theoretical. On the other hand, there are several studies on the OH reaction with methyl-*t*-butylether (MtBE). The reported kinetic data was

* Authors to whom correspondence should be addressed. E-mail: agalano@prodigy.net.mx (A.G.), gmerino@quijote.ugto.mx (G.M.).
[†] Universidad de Guanajuato.
[‡] Universidad Nacional Autónoma de México.
[§] Universidad Autónoma Metropolitana-Iztapalapa.

10.1021/jp906144d CCC: $40.75
Published on Web 11/12/2009

experimentally obtained, with rate constants ranging from 2.97×10^{-12} to 3.22×10^{-12} $cm^3 \cdot molecule^{-1} \cdot s^{-1}$,[8,13,23-25] and E_a values varying from 0.27 to 0.31 $kcal \cdot mol^{-1}$.

Due to its cyclic structure, tetrahydrofuran (THF) is an interesting ether. There are three reports of the rate constant of its reaction with OH radical at 298 K,[14,26,27] ranging from 1.60×10^{-11} to 3.48×10^{-11} $cm^3 \cdot molecule^{-1} \cdot s^{-1}$, but only Moriarty et al.[26] have estimated E_a (-0.35 $kcal \cdot mol^{-1}$). This estimation was performed within the temperature range 263 −372 K. No branching ratios have been reported for this reaction.

Despite the fact that it has been established that branching ratios between different products in multichannel reactions are as important as the overall rate of reaction, in terms of practical applications and in the understanding of the fundamental mechanisms of chemical reactions,[28,29] there is a lack of information on branching ratios for the OH reaction with ethers. Actually, there is scarce information on branching ratios for VOC reactions in general. Therefore, it is the main aim of this work to estimate them for the following series of ethers: MEE, DEE, MnPE, MiPE, MiBE, MtBE, and THF. In addition, since there is no kinetic data available for the OH reaction with MnPE, MiPE, and MiBE, it is also our purpose to provide it here.

Computational Details

Full geometry optimizations, frequency calculations, and intrinsic reaction coordinate (IRC)[30] calculations were performed with the Gaussian 03[31] program. Unrestricted calculations were used for open shell systems. The stability of the wave functions was tested, and in all the cases they were found to be stable. Local minima and transition states were identified by the number of imaginary frequencies (NIMAG = 0 or 1, respectively). IRC calculations were carried out at the corresponding level of theory in order to confirm that the transition states structures connected the proper reactants and products. The paths have been computed by following the Gonzalez−Schlegel steepest descent path,[32] in mass-weighted internal coordinates. One hundred points were modeled on each side of the saddle points, with a 0.01 $amu^{1/2} \cdot bohr$ gradient step size. Energy thermodynamic corrections at 298.15 K were included for the energy barriers and reaction heats calculations.

The rate constants have been computed using the interpolated variational transition-state theory by mapping (IVTST-M),[33] as implemented in POLYRATE 9.1 code.[34] In the IVTST-M algorithm the calculations of rate constants evaluated by canonical variational theory (CVT)[35] with small-curvature tunneling (SCT) corrections based on reaction-path data. The energies, energy gradients, and Hessians are computed at a small number of points along the minimum free energy path (MEP) and fitted to splines under tension as functions of a mapped independent variable that is a nonlinear function of the reaction coordinate.[33] The notation IVTST-M-*H*/*G* means that interpolations are based on optimized calculations of stationary points (reactants, reactant complex, transition state, product complex, and product) plus *G* additional energies and gradients, and *H* additional Hessians corresponding to nonstationary points on the MEP. In the present work all the rate constant calculations were performed using the IVTST-M-4/4 scheme. This approach has been chosen due to its proven reliability to reproduce rate constants of similar quality of those obtained from CVT at a much lower computational cost.[33,37] This advantage is particularly important in the present study due to the large amount of calculations that have been carried out. All the dynamic calculations employ redundant internal coordinates for generalized normal-mode analyses.[38] We have used a step size of $0.01a_0$ for all IVTST-M calculations

TABLE 1: Overall Rate Coefficients at 298 K (k^{298}, $cm^3 \cdot molecule^{-1} \cdot s^{-1}$) and Arrhenius Activation Energies (E_a, $kcal \cdot mol^{-1}$) for the OH + DME Gas Phase Reaction

Computational Method	k^{298}	E_a
BHandHLYP/6-311++G(d,p)	3.09×10^{-14}	3.09
CCSD(T)/6-311++G(2d,2p)//BHandHLYP/6-311++G(d,p)	1.36×10^{-12}	1.37
M05−2X/6-311++G(d,p)	4.44×10^{-12}	0.98
CCSD(T)/6-311++G(2d,2p)//M05−2X/6-311++G(d,p)	2.13×10^{-13}	2.42
MP2/6-311++G(d,p)	6.34×10^{-15}	4.39
CCSD(T)/6-311++G(2d,2p)//MP2/6-311++G(d,p)	3.16×10^{-13}	2.40
recommended[41]	2.89×10^{-12}	0.74

Since accurate rate constant calculations require the proper computation of the partition functions (Q), the hindered rotor approximation has been used to correct the Q^s corresponding to internal rotations with torsional barriers comparable to RT. Direct inspection of the low-frequency modes of the studied stationary points indicates that some of them belong to hindered rotations and because of that, should be treated as hindered rotors.[39] To make this correction, these modes were removed from the vibrational partition function of the corresponding specie and replaced by the hindered rotor partition function (Q^{HR}). In our calculations we have adopted the analytical approximation to Q^{HR} for a one-dimensional hindered internal rotation proposed by Ayala and Schlegel:[40]

Different levels of theory were tested for the OH reaction with the smallest of the studied ethers (DME), all of them in conjunction with the same basis set: 6-311++G(d,p). The calculated kinetic data was then compared with the reported experimental results (Table 1). The calculations that best agree with the values recommended by Atkinson et al.[41] are those obtained with the M05−2X hybrid meta GGA functional (Figure 1). The M05−2X rate coefficient at 298 K was found to be 1.5 times higher than the recommended one, while the second best value (CCSD(T)//BHandHLYP) is 2.1 times lower. M05−2X is also the method that best describes the Arrhenius activation energy (E_a). The E_a value computed with this functional is only 0.24 $kcal \cdot mol^{-1}$ higher than the recommended value. As for the overall rate coefficient, the second best agreement for E_a was obtained with the CCSD(T)//BHandHLYP level of theory. In this case the calculated value is 0.64 $kcal \cdot mol^{-1}$ higher than the recommended one. On the basis of these results, the OH reactions for the whole set of studied ethers were computed at the M05−2X/6-311++G(d,p) level of theory. This functional has been optimized to reproduce a large kinetics database that includes both forward and reverse barrier heights and reaction energies.[42] It has been shown that this functional yields good results for thermochemistry, thermochemical kinetics, hydrogen bonding, and weak interactions, and that it also gives excellent saddle point geometries for a variety of chemical systems.[42−47]

Results and Discussion

The OH radical reactions with eight different ethers have been studied in the present work. Every possible reaction path has been taken into account:

Dimethylether (DME):

$$CH_3OCH_3 + OH \rightarrow CH_3OCH_2 + H_2O$$

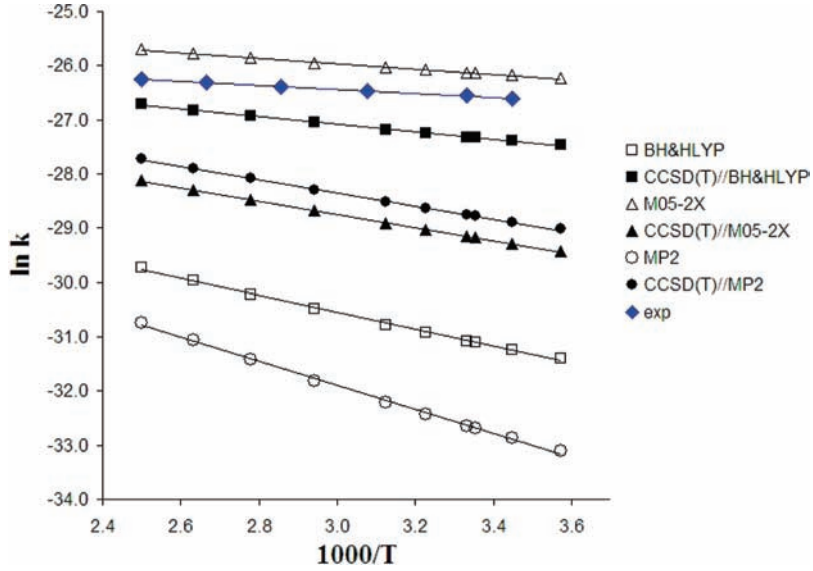

Figure 1. Comparison of computed and experimental[41] Arrhenius plots for the ·OH + DME reaction within the 280−400 K temperature range.

Methylethylether (MEE):

$$CH_3OCH_2CH_3 + OH \rightarrow CH_2OCH_2CH_3 + H_2O \quad \text{Path A}$$

$$CH_3OCH_2CH_3 + OH \rightarrow CH_3OCHCH_3 + H_2O \quad \text{Path B}$$

$$CH_3OCH_2CH_3 + OH \rightarrow CH_3OCH_2CH_2 + H_2O \quad \text{Path C}$$

Diethlylether (DEE):

$$CH_3CH_2OCH_2CH_3 + OH \rightarrow CH_2CH_2OCH_2CH_3 + H_2O \quad \text{Path A}$$

$$CH_3CH_2OCH_2CH_3 + OH \rightarrow CH_3CHOCH_2CH_3 + H_2O \quad \text{Path B}$$

Methly *n*-propylether (MnPE):

$$CH_3OCH_2CH_2CH_3 + OH \rightarrow CH_2OCH_2CH_2CH_3 + H_2O \quad \text{Path A}$$

$$CH_3OCH_2CH_2CH_3 + OH \rightarrow CH_3OCHCH_2CH_3 + H_2O \quad \text{Path B}$$

$$CH_3OCH_2CH_2CH_3 + OH \rightarrow CH_3OCH_2CHCH_3 + H_2O \quad \text{Path C}$$

$$CH_3OCH_2CH_2CH_3 + OH \rightarrow CH_3OCH_2CH_2CH_2 + H_2O \quad \text{Path D}$$

Methly *iso*-propylether (MiPE):

$$CH_3OCH(CH_3)_2 + OH \rightarrow CH_2OCH(CH_3)_2 + H_2O \quad \text{Path A}$$

$$CH_3OCH(CH_3)_2 + OH \rightarrow CH_3OC(CH_3)_2 + H_2O \quad \text{Path B}$$

$$CH_3OCH(CH_3)_2 + OH \rightarrow CH_3OCH(CH_2,CH_3) + H_2O \quad \text{Path C}$$

Methyl-*iso*-butylether (MiBE):

$$CH_3OCH_2CH(CH_3)_2 + OH \rightarrow CH_2OCH_2CH(CH_3)_2 + H_2O \quad \text{Path A}$$

$$CH_3OCH_2CH(CH_3)_2 + OH \rightarrow CH_3OCHCH(CH_3)_2 + H_2O \quad \text{Path B}$$

$$CH_3OCH_2CH(CH_3)_2 + OH \rightarrow CH_3OCH_2C(CH_3)_2 + H_2O \quad \text{Path C}$$

$$CH_3OCH_2CH(CH_3)_2 + OH \rightarrow CH_3OCH_2CH(CH_2,CH_3) + H_2O \quad \text{Path D}$$

Methyl-*ter*-butylether (MtBE):

$$CH_3OC(CH_3)_3 + OH \rightarrow CH_2OC(CH_3)_3 + H_2O \quad \text{Path A}$$

$$CH_3OC(CH_3)_3 + OH \rightarrow CH_3OC(CH_2,2CH_3) + H_2O \quad \text{Path B}$$

Tetrahydrofuran (THF):

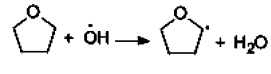

Path A

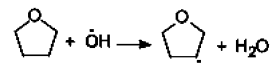

Path B

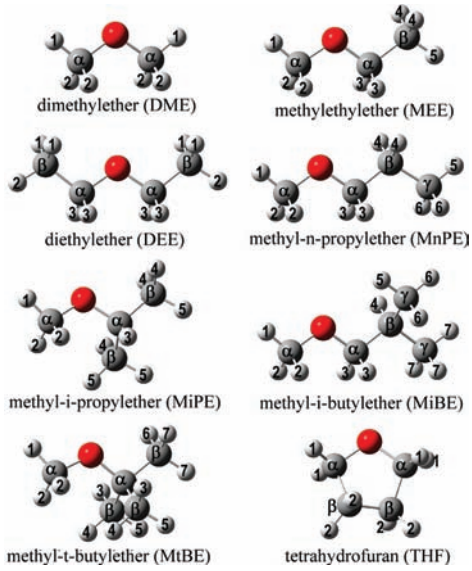

Figure 2. Studied ethers. The H atoms considered different in the modeling have been labeled accordingly.

Due to the presence of the O atom in the ethers structures not all the H, attached to the same carbon, are equivalent. The difference arises from the H arrangement with respect to the O atom. Therefore, each reaction path, above-mentioned, can take place in more than one way. This peculiarity for hydrogen abstractions from oxygenated organic compounds has been previously taken into account and accordingly applied for the OH reaction with ketones.[48,49] In this work, each reaction channel has been modeled taking into account the conformation of the abstracted H atom. Taking the O atom as the reference, two possible orientations have been considered for the transition states: (1) Syn: the hydrogen atom is in the eclipsed conformation with respect to the O atom. This orientation leads to a possible attractive interaction with the H atom in the OH radical. (2) Anti: The dihedral angle involving the H to be abstracted and the oxygen atom is between 120° and −120°. This orientation prevents possible interactions with the OH radical.

This differentiation is explicitly shown in Figure 2, where H atoms in each of the studied ethers have been accordingly labeled.

As for many other oxygenated VOCs,[50] reactant complexes (RC) were found in the entrance channel of each modeled path (Figures S1−S8 in the Supporting Information). They were obtained by optimizing the final structures from the IRC calculations, at the reactant side. This search was performed for all the transition states. In several cases, more than one channel lead to the same RC. In general, the reactant complexes (RC) formation occurs by H bond interactions between the H atom in the OH radical and the O atom in the corresponding ether. The interacting distance ($H^{OH}\cdots O^{ether}$) was found to be about 1.8 Å, and the complexes are about 7 kcal·mol^{-1} lower in enthalpy than the isolated reactants. When the reaction site is too far away from the O atom in the ether, the complexes are formed via a much weaker interaction: in these cases between the O atom in the OH, and one of the H atoms in the ether. In such cases, the $O^{OH}\cdots H^{ether}$ distance becomes significantly larger, increasing from 2.2 to 2.7 Å, and the stabilization energy becomes about 1.3 kcal·mol^{-1} lower with respect to the isolated reactants. The fully optimized geometries of the product complexes (PC), formed at the exit channel and explicitly considered for the kinetic calculations, are provided as Supporting Information (Figures S9−S16).

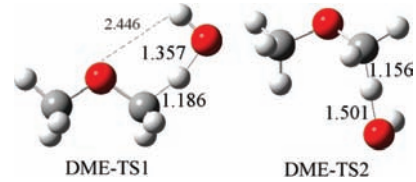

Figure 3. Different transition state structures corresponding to OH hydrogen abstractions from DME.

The influence of the orientation of the H to be abstracted (relative to the O atom in the ether) on the TS structures is clearly shown in Figure 3. Depending on this orientation, two different transition states arise. Not only their geometries are significantly different, but also their energies. It was found that the syn TS (TS1) is about 2 kcal·mol^{-1} lower than the anti one (TS2). This difference in the reaction barriers would lead to significantly different rate constants. Therefore, if just one of them is considered, and the reaction paths degeneracy is assumed to be 6, a large discrepancy would arise between the rate constants calculated this way and the observed ones. The calculated value would be significantly overestimated if only TS1 is computed, and significantly underestimated if only TS2 is considered. In this case, where this distinction has been taken into account, that is, two different channels have been computed for the DME + OH reaction, the reaction paths degeneracy becomes 2 for the syn path and 4 for the anti one.

This procedure has also been applied for the other studied ethers, therefore most of the paths mentioned above split at least into two channels that depend on the orientation of the H to be abstracted. Each of these channels corresponds to a different label in Figure 2. The transition states geometries, corresponding to ethers different than DME, are provided as Supporting Information (Figures S17−S23). Their energies, relative to that of the isolated reactants are reported in Table 2 along with the reaction energies. For the transition states, the energy difference between syn and anti TS structures is systematically larger than 1 kcal·mol^{-1}, in terms of Gibbs free energy, which represents 1 order of magnitude in terms of rate constants. The only exceptions are H(1) and H(2) abstractions from MiPE, which show similar barriers. This can be explained by their geometrical properties (Figure S19). For this particular ether, in the anti TS, the OH moiety rotates in such way that the intramolecular interaction between the H atom in the OH and the O atom in the ether, characteristic of syn TSs, becomes possible.

All reaction channels were found to be exothermic and exergonic (Table 2). For each reaction path only one product was found. Path B (channels 1 and 2) yields the product lowest in energy for MEE, which is a logical finding since it corresponds to H abstractions from the only secondary carbon in this ether. Because of the same reason, the path B products are, thermodynamically, the most favored ones for DEE. In the MnPE case, there are two secondary carbons, one directly bonded to the O atom (Path B) and one in a β position with respect to it (Path C). The radical product from the first one is lower in energy. The same behavior was found when comparing the two paths involving abstraction from primary carbon sites: the radical product where the H was abstracted from the C directly bonded to the O atom is lower in energy. Therefore, the presence of the O atom next to the abstraction site seems to stabilize the formed radical. The same trend was found for all the studied ethers. For MiPE, path B leads to the product lowest in energy since it corresponds to the H abstraction from the tertiary carbon site, which is also directly bonded to the O atom. Within this line of reasoning, MiBE is an interesting structure

since it has a secondary C atom directly bonded to the O atom (path B) and a tertiary carbon that is not (path C). Since the first one was found to be lower in energy than the second one, it can be stated that the vicinity to the O atom influences the stability of the formed radical to a larger extent than the nature of the carbon site (primary, secondary, or tertiary). In MtBE all the sites with H atoms to be abstracted correspond to primary carbons. Once again, the path leading to the product lowest in energy corresponds to abstractions from the methyl group directly bonded to the O atom (path A). The same was found for THF: path A (sites next to O) leads to the thermodynamically most favored products.

For the kinetic calculations it has been assumed that neither mixing nor crossover between different pathways occurs. Thus, the overall rate constant (k), which corresponds to the reaction of each ether with OH, is determined as the sum of each path rate coefficients,[51] and in turn, rate coefficient of each path is obtained as the sum of the corresponding channels (according to the H orientation):

$$k_{\mathrm{DME}} = k_1 + k_2 \quad (1)$$

$$k_{\mathrm{MEE}} = k_{\mathrm{A}} + k_{\mathrm{B}} + k_{\mathrm{C}} = (k_1 + k_2) + (k_3) + (k_4 + k_5) \quad (2)$$

$$k_{\mathrm{DEE}} = k_{\mathrm{A}} + \mathrm{k}_B = (k_1 + k_2) + (k_3) \quad (3)$$

$$k_{\mathrm{MnPE}} = k_{\mathrm{A}} + k_{\mathrm{B}} + k_{\mathrm{C}} + k_{\mathrm{D}} = (k_1 + k_2) + (k_3) + (k_4) + (k_5 + k_6) \quad (4)$$

$$k_{\mathrm{MiPE}} = k_{\mathrm{A}} + k_{\mathrm{B}} + k_{\mathrm{C}} = (k_1 + k_2) + (k_3) + (k_4 + k_5) \quad (5)$$

$$k_{\mathrm{MiBE}} = k_{\mathrm{A}} + k_{\mathrm{B}} + k_{\mathrm{C}} + k_{\mathrm{D}} = (k_1 + k_2) + (k_3) + (k_4) + (k_5 + k_6 + k_7) \quad (6)$$

$$k_{\mathrm{MtBE}} = k_{\mathrm{A}} + k_{\mathrm{B}} = (k_1 + k_2) + (k_3 + k_4 + k_5 + k_6 + k_7) \quad (7)$$

$$k_{\mathrm{THF}} = k_{\mathrm{A}} + k_{\mathrm{B}} = (k_1) + (k_2) \quad (8)$$

Each k_i, with $i = \{1,2, ...\}$, has been computed with the IVTST-M, as previously described in the Computational Details section.

Since we are interested in the details of the studied reactions under tropospheric conditions, particularly for the lower troposphere, we will focus our discussion on the results obtained in the 280−400 K temperature range. This is also the range for which most experimental data is available. However, additional information is provided as Supporting Information up to 2000 K (Table S9). The overall rate coefficients for the OH reactions with all the studied ethers are reported in Table 3. Calculated values at 298.15 K have been highlighted in bold characters, and experimental ones at the same temperature in italic characters. The agreement with the available experimental data (DME, MEE, DEE, MtBE, and THF) is very good. The calculated values differ from the experimental ones by a factor of 2 at the most, for THF. This excellent agreement supports the reliability of the rate coefficients proposed here for the first time for MnPE, MiPE, and MiBE. In addition, in order to assess the importance of using the variational TST for calculating the rate constants, the values obtained from conventional TST are also reported in Table 3. The first, and logical, finding is that the rate constants obtained with conventional TST are systematically higher. However, the most important comparison is related to the agreement with the available experimental data. This agreement is better when variational theory is used for the kinetic calculations. The mean unsigned error for ln(k), with respect to the experiments at 298 K, was found to be equal to 2.6 and 4.8 for rate constants computed with variational and conventional transition states theories, respectively. However, this strongly depends on temperature. The ratio $k^{\mathrm{TST}}/k^{\mathrm{IVTST\text{-}M}}$, which is a measurement of the importance of taking into account the variational effects on kinetic calculations, is reported in Supporting Information Table S10. As this table show, as the temperature raises the rate constants computed with both approaches become closer, that is, the lower the temperature the more important the variational effect.

The branching ratios (Γ) for the different paths contributing to the overall reactions, at 298.15 K, are reported in Table 4. More detailed data, differentiating between H atoms at each site, and for the whole set of studied temperatures, are provided as Supporting Information (Tables S1−S8). In every case, the branching ratios are expressed as an overall rate coefficients percentage. For MEE the reaction path contributing the most to the overall reaction is path B, with contributions from 68.3% at 280 K to 60.5% at 400 K. Path C gives only minor contribution. Albeit its importance increases with temperature,

TABLE 2: Reaction Energies and Reaction Barriers, Relative to Isolated Reactants (in kcal·mol^{-1})

		ΔE^a	ΔH^b	ΔG^b	$\Delta E‡^a$	$\Delta H‡^b$	$\Delta G‡^b$
DME	(1)	−21.95	−21.53	−22.83	1.69	1.04	9.02
	(2)				−0.07	−0.89	7.57
MEE	(1)	−21.77	−21.37	−22.77	1.95	1.23	9.27
	(2)				0.33	−0.55	8.18
	(3)	−23.02	−22.56	−24.00	−0.76	−1.59	7.28
	(4)	−15.51	−15.00	−16.50	0.41	−0.72	8.94
	(5)				3.22	2.56	10.59
DEE	(1)	−15.66	−15.19	−16.59	−0.22	−1.21	8.00
	(2)				2.83	2.23	10.13
	(3)	−23.40	−22.92	−24.53	−1.29	−2.05	6.66
MnPE	(1)	−21.96	−21.56	−22.91	1.53	0.91	7.39
	(2)				−0.20	−0.95	7.42
	(3)	−23.00	−22.56	−24.12	−1.42	−2.24	6.71
	(4)	−19.06	−18.45	−20.54	−1.86	−2.78	6.33
	(5)	−17.15	−16.59	−18.46	2.45	1.77	9.94
	(6)				1.74	0.97	9.56
MiPE	(1)=(2)	−22.73	−22.28	−23.55	−0.23	−0.98	7.66
	(3)	−23.22	−22.81	−24.12	−1.53	−2.34	6.76
	(4)	−15.60	−14.92	−17.34	2.45	1.77	10.22
	(5)				−0.16	−1.13	8.18
MiBE	(1)	−21.68	−21.38	−22.36	2.09	1.28	10.06
	(2)				0.12	−0.76	8.19
	(3)	−22.36	−21.92	−23.58	−1.43	−2.18	6.77
	(4)	−16.47	−15.97	−17.57	−3.00	−3.95	5.73
	(5)				−1.02	−2.09	7.62
	(6)	−20.27	−19.63	−21.98	0.62	−0.44	9.33
	(7)				1.53	0.71	9.63
MtBE	(1)	−22.74	−22.50	−22.86	1.22	0.35	9.50
	(2)				−0.11	−0.91	8.02
	(3)	−16.60	−16.15	−17.08	−0.56	−1.64	8.49
	(4)				1.48	0.65	9.77
	(5)				1.90	1.10	10.44
	(6)	−15.04	−14.40	−16.47	−0.65	−1.69	8.35
	(7)				2.00	1.23	10.21
THF	(1)	−24.30	−24.08	−24.63	−1.39	−2.22	6.69
	(2)	−20.21	−19.86	−20.67	−0.45	−1.49	8.19

[a] Including ZPE corrections [b] At 298.15 K.

TABLE 3: Overall Rate Coefficients ($cm^3 \cdot molecule^{-1} \cdot s^{-1}$) Corresponding to the OH Reactions with the Studied Ethers

T	DME	MEE	DEE	MnPE	MiPE	MiBE	MtBE	THF
				IVTST-M/SCT				
280.00	4.06×10^{-12}	2.53×10^{-12}	1.36×10^{-11}	1.20×10^{-11}	6.83×10^{-12}	8.93×10^{-12}	1.48×10^{-12}	3.82×10^{-11}
290.00	4.27×10^{-12}	2.67×10^{-12}	1.38×10^{-11}	1.22×10^{-11}	6.95×10^{-12}	8.83×10^{-12}	1.57×10^{-12}	3.78×10^{-11}
298.15	$\mathbf{4.44 \times 10^{-12}}$	$\mathbf{2.78 \times 10^{-12}}$	$\mathbf{1.40 \times 10^{-11}}$	$\mathbf{1.23 \times 10^{-11}}$	$\mathbf{7.09 \times 10^{-12}}$	$\mathbf{8.78 \times 10^{-12}}$	$\mathbf{1.64 \times 10^{-12}}$	$\mathbf{3.76 \times 10^{-11}}$
300.00	4.49×10^{-12}	2.81×10^{-12}	1.40×10^{-11}	1.23×10^{-11}	7.13×10^{-12}	8.78×10^{-12}	1.66×10^{-12}	3.75×10^{-11}
310.00	4.71×10^{-12}	2.95×10^{-12}	1.42×10^{-11}	1.25×10^{-11}	7.28×10^{-12}	8.76×10^{-12}	1.75×10^{-12}	3.73×10^{-11}
320.00	4.93×10^{-12}	3.09×10^{-12}	1.44×10^{-11}	1.27×10^{-11}	7.45×10^{-12}	8.77×10^{-12}	1.85×10^{-12}	3.70×10^{-11}
340.00	5.39×10^{-12}	3.38×10^{-12}	1.48×10^{-11}	1.31×10^{-11}	7.81×10^{-12}	8.93×10^{-12}	2.05×10^{-12}	3.66×10^{-11}
360.00	5.87×10^{-12}	3.71×10^{-12}	1.54×10^{-11}	1.38×10^{-11}	8.24×10^{-12}	9.40×10^{-12}	2.27×10^{-12}	3.62×10^{-11}
380.00	6.37×10^{-12}	4.06×10^{-12}	1.60×10^{-11}	1.46×10^{-11}	8.74×10^{-12}	9.88×10^{-12}	2.51×10^{-12}	3.60×10^{-11}
400.00	6.90×10^{-12}	4.42×10^{-12}	1.68×10^{-11}	1.54×10^{-11}	9.28×10^{-12}	1.04×10^{-11}	2.80×10^{-12}	3.59×10^{-11}
				TST/ZCT				
280.00	1.61×10^{-11}	1.05×10^{-11}	4.90×10^{-11}	4.27×10^{-11}	1.69×10^{-11}	4.53×10^{-11}	4.08×10^{-12}	3.84×10^{-11}
290.00	1.61×10^{-11}	1.05×10^{-11}	4.72×10^{-11}	4.08×10^{-11}	1.65×10^{-11}	4.10×10^{-11}	4.15×10^{-12}	3.80×10^{-11}
298.15	1.59×10^{-11}	1.05×10^{-11}	4.60×10^{-11}	3.94×10^{-11}	1.62×10^{-11}	3.82×10^{-11}	4.21×10^{-12}	3.78×10^{-11}
300.00	1.60×10^{-11}	1.05×10^{-11}	4.57×10^{-11}	3.92×10^{-11}	1.61×10^{-11}	3.76×10^{-11}	4.23×10^{-12}	3.77×10^{-11}
310.00	1.60×10^{-11}	1.05×10^{-11}	4.43×10^{-11}	3.78×10^{-11}	1.58×10^{-11}	3.48×10^{-11}	4.33×10^{-12}	3.75×10^{-11}
320.00	1.60×10^{-11}	1.05×10^{-11}	4.31×10^{-11}	3.68×10^{-11}	1.56×10^{-11}	3.25×10^{-11}	4.42×10^{-12}	3.72×10^{-11}
340.00	1.61×10^{-11}	1.06×10^{-11}	4.12×10^{-11}	3.50×10^{-11}	1.53×10^{-11}	2.97×10^{-11}	4.63×10^{-12}	3.68×10^{-11}
360.00	1.64×10^{-11}	1.09×10^{-11}	4.01×10^{-11}	3.53×10^{-11}	1.52×10^{-11}	2.92×10^{-11}	4.87×10^{-12}	3.64×10^{-11}
380.00	1.67×10^{-11}	1.12×10^{-11}	3.96×10^{-11}	3.60×10^{-11}	1.55×10^{-11}	2.88×10^{-11}	5.21×10^{-12}	3.62×10^{-11}
400.00	1.71×10^{-11}	1.15×10^{-11}	3.94×10^{-11}	3.68×10^{-11}	1.58×10^{-11}	2.84×10^{-11}	5.71×10^{-12}	3.60×10^{-11}
Exp 298.15	*2.77×10^{-12}* [41]	*5.09×10^{-12}* [41]	*1.32×10^{-11}* [21]	NA	NA	NA	3.10×10^{-12} [26]	1.80×10^{-11} [26]

TABLE 4: Branching Ratios (Γ) at 298.15 K

	Γ (A)	Γ (B)	Γ (C)	Γ (D)
MEE	29.80	67.34	2.86	
DEE	3.62	96.38		
MnPE	30.64	57.98	10.65	0.73
MiPE	46.36	49.05	4.60	
MiBE	9.71	50.78	22.45	17.06
MtBE	73.57	26.43		
THF	96.47	3.53		

TABLE 5: Arrhenius Parameters in the 280−400 K Range

	A ($cm^3 \cdot molec^{-1} \cdot s^{-1}$)	E_a ($kcal \cdot mol^{-1}$)
DME	2.34×10^{-11}	0.98
MEE	1.58×10^{-11}	1.02
DEE	2.63×10^{-11}	0.37
MnPE	2.65×10^{-11}	0.45
MiPE	1.83×10^{-11}	0.56
MiBE	1.41×10^{-11}	0.28
MtBE	1.19×10^{-11}	1.17
THF	3.08×10^{-11}	−0.12

up to 400 K its contribution remains below 5%. Path B is also the main path for the OH + DEE reaction. In this case its contribution to the overall reaction rate ranges from 96.5% at 280 K to 93.5% at 400 K. Even though for the MnPE + OH reaction path B remains the major one, a large product distribution is expected since three different paths make significant contribution to the overall reaction: paths A, B, and C. Although Γ(B) decreases with temperature, it remains as the path contributing the most to the overall reaction, at least up to 400 K. For MiPE, on the other hand, the branching ratios of paths A and B are very similar to each other within the analyzed temperature range. However, as the temperature rises Γ(A) increases while Γ(B) decreases. These opposite trends make B the path contributing the most to the overall reaction up to 300 K, whereas path A becomes the main path at higher temperatures. Path C contributions are less than 10% within the whole temperature range. The main path of reaction for MiBE was found to be path B, while for MtBE and THF path A shows the largest contributions to the overall rate constants.

The influence of temperature on the rate of the chemical reactions studied in this work has been interpreted first in terms of the Arrhenius equation:[52]

$$k = Ae^{-E_a/RT} \tag{9}$$

where *A* is known as the pre-exponential factor and E_a represents the activation energy. In eq 9 the influence of the temperature is accounted for in the exponential part of the expression. Since the Arrhenius equation is probably the expression most widely used to interpret kinetic data, it is convenient to use it for the analysis of the temperature dependence of rate constants, taking into account possible further comparisons. The parameters corresponding to the best linear fittings are reported in Table 5.

As Figure 4 shows, the Arrhenius plots for the overall rate coefficients are not linear, particularly for DEE, MnPE, MiPE, and MiBE, demonstrating that activation energy changes with temperature within 280−400 K. Since the activation energies vary within the studied temperature range, the Arrhenius equation is not the most convenient expression to describe the temperature influence on the corresponding rate coefficients. A

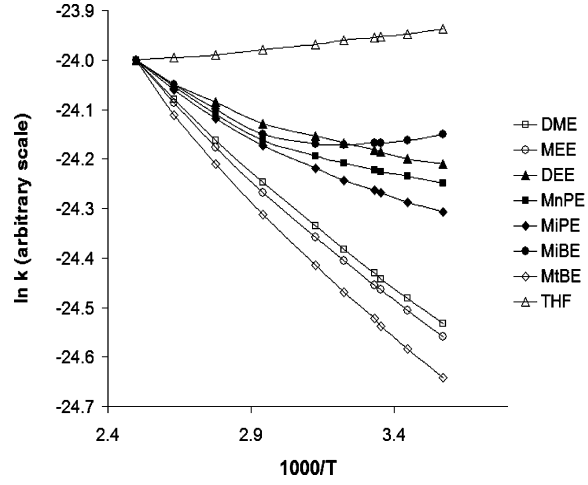

Figure 4. Arrhenius plots for the OH reactions with the studied ethers, in the 280−400 K range.

TABLE 6: Kooij Parameters in the 280−400 K Temperature Range

	B ($cm^3 \cdot molec^{-1} \cdot s^{-1}$)	m	E_0 ($kcal \cdot mol^{-1}$)
DME	2.0×10^{-16}	1.71	−0.15
MEE	9.0×10^{-19}	2.44	−0.58
DEE	5.3×10^{-18}	2.26	−1.12
MnPE	1.6×10^{-21}	3.44	−1.82
MiPE	7.2×10^{-20}	2.84	−1.31
MiBE	5.4×10^{-28}	5.55	−3.37
MtBE	4.0×10^{-20}	2.86	−0.72
THF	3.3×10^{-12}	0.33	−0.33

TABLE 7: Activation Energies ($kcal \cdot mol^{-1}$) as a Function of Temperature (from Kooij Fit)

T	DME	MEE	DEE	MnPE	MiPE	MiBE	MtBE	THF
280.00	0.80	0.78	0.14	0.09	0.27	−0.28	0.87	−0.15
290.00	0.84	0.83	0.18	0.16	0.33	−0.17	0.93	−0.14
298.15	0.86	0.87	0.22	0.22	0.37	−0.08	0.97	−0.13
300.00	0.87	0.87	0.23	0.23	0.38	−0.06	0.98	−0.13
310.00	0.90	0.92	0.27	0.30	0.44	0.05	1.04	−0.13
320.00	0.94	0.97	0.32	0.37	0.50	0.16	1.10	−0.12
340.00	1.01	1.07	0.41	0.50	0.61	0.38	1.21	−0.11
360.00	1.07	1.17	0.50	0.64	0.72	0.60	1.33	−0.09
380.00	1.14	1.26	0.59	0.78	0.83	0.82	1.44	−0.08
400.00	1.21	1.36	0.68	0.91	0.95	1.04	1.55	−0.07

more general procedure, commonly used to analyze data in such cases, is fitting the data with the equation proposed by Kooij:[53]

$$k = BT^m e^{-E_0/RT} \quad (10)$$

where B, E_0, and m are independent temperature parameters. After that the activation energy can be calculated as function of temperature, as:

$$E_a(T) = E_0 + mRT \quad (11)$$

where E_0 is the hypothetical activation energy at 0 K.

It could be interesting to discuss the variation of the activation energies with temperature (Table 7). The Kooij overall activation energy was found to increase as temperature rises for all the studied ethers. $E_a(T)$ is negative in the 280−400 K range for THF and for temperatures lower than 300 K for MiBE, and positive in all the other cases. The largest variation of $E_a(T)$ was found for MiBE (1.32 kcal mol^{-1} from 280 to 400 K), while THF shows the smallest variation. In fact, for THF the influence of temperature on the activation energy is negligible, at least from 280 to 400 K, that is, it only changes by 0.08 $kcal \cdot mol^{-1}$ within this range. These results indicate that the tropospheric reactivity toward OH radicals increases with height for all the studied ethers, with the exception of THF.

Conclusions

The M05−2X functional has been proven to accurately reproduce the experimental data available for ethers + OH reactions. For the DME + OH reaction in particular it was shown to perform better than some very reliable wavefunction methods such as CCSD(T)//MP2.

A stepwise mechanism is proposed for the OH reaction with all the studied ethers. It involves the formation of reactant complexes in the entrance channel and product complexes in the exit channels.

The importance of differentiating among the H atoms at each site of reaction, according to their orientation with respect to the O atom in the ether, is analyzed. It was found that if such differentiation is not taken into account the accuracy of the kinetic data would be seriously affected.

Branching ratios indicate that the presence of the O atom in the vicinity of the H abstraction site increases its reactivity toward OH radicals. This influence was found to be even larger than that of the nature of the carbon site (primary, secondary, tertiary).

The overall agreement between the calculated and the available experimental data is very good and supports the reliability of the rate coefficients and the branching ratios proposed here for the first time.

Acknowledgment. A.G. thanks Laboratorio de Visualización y Cómputo Paralelo at UAM - Iztapalapa for the access to its computer facilities. J.R.A.-I. thanks the Dirección General de Servicios de Cómputo Académico (DGSCA) at Universidad Nacional Autónoma de México. This work was partially supported by a grant from the DGAPA UNAM (PAPIIT-IN203808). The work in Guanajuato was funded by Conacyt (Grant 57892). C.Z.-O. acknowledges CONACyT for the Master fellowship. C.Z.-O. and G.M. thank Maryel Contreras for valuable discussion.

Supporting Information Available: Optimized geometries of reactant complexes, product complexes, and transition states. Branching ratios for all modeled channels, within the 280−400 K temperature range. Rate coefficients from 400 to 2000 K. $k^{TST}/k^{IVTST\text{-}M}$ ratio in the 280−2000 K temperature range. This material is available free of charge via the Internet at http://pubs.acs.org.

References and Notes

(1) Guidance on Estimating Motor Vehicle Emission Reductions from the Use of Alternative Fuels and Fuel Blends, Report No. EPA-AA-TSS-PA-874; US. EPA: Ann Arbor, Michigan, 1988.
(2) Ramadhas, A. S.; Jayaraj, S.; Muraleedharan, C. *Int. J. Global Ener. Issues* **2008**, *29*, 329.
(3) Atkinson, R. Atmospheric Transformations of Automotive Emissions. In *Air Pollution, the Automobile, and Public Health*; Watson, A. Y., Bates, R. R., Kennedy, D., Eds.; National Academy Press: Washington, DC, 1988; pp 99−132.
(4) Atkinson, R. *J. Phys. Chem. Ref. Data* **1994**, Monograph *2*, 1.
(5) Calvert, J.; Pitts Jr., J. N. *Photochemistry*; Wiley: New York, 1966.
(6) Atkinson, R.; Carter, W. P. L. *Chem. Rev.* **1984**, *84*, 437.
(7) Wallington, T. J.; Atkinson, R.; Winer, A. M.; Pitts, J. N, Jr. *J. Phys. Chem.* **1986**, *90*, 5393.
(8) Bonard, A.; Daele, V.; Delfau, J.-L.; Vovelle, C *J. Phys. Chem. A* **2002**, *106*, 4384.
(9) DeMore, W. B.; Bayes, K. D. *J. Phys. Chem. A* **1999**, *103*, 2649.
(10) Arif, M.; Dellinger, B.; Taylor, P. H. *J. Phys. Chem. A* **1997**, *101*, 2436.
(11) Mellouki, A.; Teton, S.; LeBras, G. *Int. J. Chem. Kinet.* **1995**, *27*, 791.
(12) Nelson, L.; Rattigan, O.; Neavyn, R.; Sidebottom, H.; Treacy, J.; Nielsen, O. J. *Int. J. Chem. Kinet.* **1990**, *22*, 1111.
(13) Wallington, T. J.; Andino, J. M.; Skewes, L. M.; Siegl, W. O.; Japar, S. M. *Int. J. Chem. Kinet.* **1989**, *21*, 993.
(14) Wallington, T. J.; Liu, R.; Dagaut, P.; Kurylo, M. J. *Int. J. Chem. Kinet.* **1988**, *20*, 41.
(15) Tully, F. P.; Droege, A. T. *Int. J. Chem. Kinet.* **1987**, *19*, 251.
(16) Perry, R. A.; Atkinson, R.; Pitts, J. N, Jr. *J. Chem. Phys.* **1977**, *67*, 611.
(17) Wu, J. Y.; Liu, J. Y.; Li, Z. S.; Sun, C. C. *J. Chem. Phys.* **2003**, *118*, 10986.
(18) Urata, S.; Takada, A.; Uchimaru, T.; Chandra, A. K. *Chem. Phys. Lett.* **2003**, *368*, 215.
(19) Starkey, D. P.; Holbrook, K. A.; Oldershaw, G. A.; Walker, R. W. *Int. J. Chem. Kinet.* **1997**, *29*, 231.
(20) Yang, L.; Liu, J. Y.; Wang, L.; He, H. Q.; Wang, Y.; Li, Z. S. *J. Comput. Chem.* **2008**, *29*, 550.
(21) Semadeni, M.; Stocker, D. W.; Kerr, J. A. *J. Atmos. Chem.* **1993**, *16*, 79.

(22) Bennett, P. J.; Kerr, J. A. *J. Atmos. Chem.* **1989**, *8*, 87.

(23) Picquet, B.; Heroux, S.; Chebbi, A.; Doussin, J.-F.; Durand-Jolibois, R.; Monod, A.; Loirat, H.; Carlier, P. *Int. J. Chem. Kinet.* **1998**, *30*, 839.

(24) Teton, S.; Mellouki, A.; LeBras, G.; Sidebottom, H. *Int. J. Chem. Kinet.* **1996**, *28*, 291.

(25) Smith, D. F.; Kleindienst, T. E.; Hudgens, E. E.; McIver, C. D.; Bufalini, J. J. *Int. J. Chem. Kinet.* **1991**, *23*, 907.

(26) Moriarty, J.; Sidebottom, H.; Wenger, J.; Mellouki, A.; Le Bras, G. *J. Phys. Chem. A* **2003**, *107*, 1499.

(27) Ravishankara, A. R.; Davis, D. D. *J. Phys. Chem.* **1978**, *82*, 2852.

(28) Seakins, P. W. *Annu. Rep. Prog. Chem., Sect. C: Phys. Chem.* **2007**, *103*, 173.

(29) (a) Butkovskaya, N. I.; Kukui, A.; Le Bras, G. *J. Phys. Chem. A* **2004**, *108*, 1160. (b) Butkovskaya, N. I.; Setser, D. W. *J. Phys. Chem. A.* **1999**, *103*, 6921. (c) Butkovskaya, N. I.; Kukui, A.; Pouvesle, N.; Le Bras, G. *J. Phys. Chem. A.* **2004**, *108*, 7021.

(30) Gonzalez, C.; Schlegel, H. B. *J. Phys. Chem.* **1990**, *94*, 5523.

(31) Frisch, M. J.; Trucks, G. W.; Schlegel, H. B.; Scuseria, G. E.; Robb, M. A.; Cheeseman, J. R.; Montgomery, Jr., J. A.; Vreven, T.; Kudin, K. N.; Burant, J. C.; Millam, J. M.; Iyengar, S. S.; Tomasi, J.; Barone, V.; Mennucci, B.; Cossi, M.; Scalmani, G.; Rega, N.; Petersson, G. A.; Nakatsuji, H.; Hada, M.; Ehara, M.; Toyota, K.; Fukuda, R.; Hasegawa, J.; Ishida, M.; Nakajima, T.; Honda, Y.; Kitao, O.; Nakai, H.; Klene, M.; Li, X.; Knox, J. E.; Hratchian, H. P.; Cross, J. B.; Bakken, V.; Adamo, C.; Jaramillo, J.; Gomperts, R.; Stratmann, R. E.; Yazyev, O.; Austin, A. J.; Cammi, R.; Pomelli, C.; Ochterski, J. W.; Ayala, P. Y.; Morokuma, K.; Voth, G. A.; Salvador, P.; Dannenberg, J. J.; Zakrzewski, V. G.; Dapprich, S.; Daniels, A. D.; Strain, M. C.; Farkas, O.; Malick, D. K.; Rabuck, A. D.; Raghavachari, K.; Foresman, J. B.; Ortiz, J. V.; Cui, Q.; Baboul, A. G.; Clifford, S.; Cioslowski, J.; Stefanov, B. B.; Liu, G.; Liashenko, A.; Piskorz, P.; Komaromi, I.; Martin, R. L.; Fox, D. J.; Keith, T.; Al-Laham, M. A.; Peng, C. Y.; Nanayakkara, A.; Challacombe, M.; Gill, P. M. W.; Johnson, B.; Chen, W.; Wong, M. W.; Gonzalez, C.; Pople, J. A. *Gaussian 03, Revision D.01*; Gaussian, Inc.: Wallingford CT, 2004.

(32) (a) Gonzalez, C.; Schlegel, H. B. *J. Chem. Phys.* **1989**, *90*, 2154. (b) Gonzalez, C.; Schlegel, H. B *J. Phys. Chem.* **1990**, *94*, 5523.

(33) Corchado, J. C.; Coitiño, E. L.; Chuang, Y.-Y.; Fast, P. L.; Truhlar, D. G. *J. Phys. Chem. A* **1998**, *102*, 2424.

(34) Corchado, J. C.; Chuang, Y.-Y.; Fast, P. L.; Villà, J.; Hu, W.-P.; Liu, Y.-P.; Lynch, G. C.; Nguyen, K. A.; Jackels, C. F.; Melissas, V. S.; Lynch, B. J.; Rossi, I.; Coitiño, E. L.; Fernandez-Ramos, A.; Pu, J.; Albu, T. V.; Steckler, R.; Garrett, B. C.; Isaacson, A. D.; Truhlar, D. G. *POLYRATE*, version 9.1; University of Minnesota: Minneapolis, 2002.

(35) (a) Isaacson, A. D.; Truhlar, D. G. *J. Chem. Phys.* **1982**, *76*, 1380. (b) Truhlar, D. G.; Garrett, B. C. *Annu. Rev. Phys. Chem.* **1984**, *35*, 159. (c) Chuang, Y.-Y.; Cramer, C. J.; Truhlar, D. G. *Int. J. Quantum Chem.* **1998**, *70*, 887.

(36) (a) Garrett, B. C.; Truhlar, D. G.; Grev, R. S.; Magnuson, A. W. *J. Phys. Chem.* **1980**, *84*, 1730. (b) Truhlar, D. G.; Garrett, B. C. *Annu. Rev. Phys. Chem.* **1984**, *35*, 159. (c) Truhlar, D. G.; Liu, Y.-P.; Schenter, G. K.; Garrett, B. C. *J. Phys. Chem.* **1994**, *98*, 8396.

(37) Zavala-Oseguera, C.; Galano, A. *J. Chem. Theory Comput.* **2009**, *5*, 1295.

(38) Chuang, Y.-Y.; Truhlar, D. G. *J. Phys. Chem. A* **1998**, *102*, 242.

(39) Jacox, M. E. *Vibrational and Electronic Energy Levels of Polyatomic Transient Molecules*; NIST: Gaithersburg, MD, 1998; Vol *69*.

(40) Ayala, P. Y.; Schlegel, H. B. *J. Chem. Phys.* **1998**, *108*, 2314.

(41) Atkinson, R.; Baulch, D. L.; Cox, R. A.; Hampson, R. F., Jr.; Kerr, J. A.; Rossi, M. J.; Troe, J. *J. Phys. Chem. Ref. Data* **1997**, *26*, 521.

(42) Zhao, Y.; Truhlar, D. G. *J. Phys. Chem. A* **2004**, *108*, 6908.

(43) Zhao, Y.; Schultz, N. E; Truhlar, D. G. *J. Chem. Theory Comput.* **2006**, *2*, 364.

(44) Zhao, Y.; Truhlar, D. G. *J. Phys. Chem. A* **2005**, *109*, 5656.

(45) Zhao, Y.; Truhlar, D. G. *J. Chem. Theory Comput.* **2005**, *1*, 415.

(46) Zhao, Y.; Gonzalez-Garcia, N.; Truhlar, D. G *J. Phys. Chem. A* **2005**, *109*, 2012.

(47) Vega-Rodriguez, A.; Alvarez-Idaboy, J. R. *Phys. Chem. Chem. Phys.* **2009**, *11*, 7649.

(48) Masgrau, L.; Gonzalez-Lafont, A.; Lluch, J. M. *J. Phys. Chem. A* **2002**, *106*, 11760.

(49) Alvarez-Idaboy, J. R.; Cruz-Torres, A.; Galano, A.; Ruiz-Santoyo, M. E. *J. Phys. Chem. A.* **2004**, *108*, 2740.

(50) See for example: (a) Galano, A.; Alvarez-Idaboy, J. R. *Adv. Quantum Chem.* **2008**, *55*, 245. (b) Galano, A. *J. Phys. Chem. A.* **2006**, *110*, 9153. (c) Galano, A.; Alvarez-Idaboy, J. R.; Ruiz-Santoyo, M. E.; Vivier-Bunge, A. *J. Phys. Chem. A.* **2005**, *109*, 169. (d) Galano, A.; Alvarez-Idaboy, J. R.; Ruiz-Santoyo, M. E.; Vivier-Bunge, A. *ChemPhysChem.* **2004**, *5*, 1379. (e) Galano, A.; Alvarez-Idaboy, J. R.; Bravo-Perez, G.; Ruiz-Santoyo, M. E. *Phys. Chem. Chem. Phys.* **2002**, *4*, 4648. (f) Galano, A.; Alvarez-Idaboy, J. R.; Ruiz-Santoyo, M. E.; Vivier-Bunge, A. *J. Phys. Chem. A* **2002**, *106*, 9520. (g) Mora-Diez, N.; Alvarez-Idaboy, J. R.; Boyd, R. J. *J. Phys. Chem. A* **2001**, *105*, 9034. (h) Alvarez-Idaboy, J. R.; Mora-Diez, N.; Boyd, R. J.; Vivier-Bunge, A. *J. Am. Chem. Soc.* **2001**, *123*, 2018.

(51) Robinson, P. J.; Holbrook, K. A. *Unimolecular Reactions*; Wiley-Interscience: London, 1972.

(52) Arrhenius, S. *Z. Phys. Chem.* **1889**, *4*, 226.

(53) Kooij, D. M. *Z. Phys. Chem.* **1893**, *12*, 155.

JP906144D